AIP Journal of Applied Physics

Experimental and theoretical analysis of the temperature dependence of the two-dimensional electron mobility in a strained Si quantum well

Takahisa Tanaka, Go Tsuchiya, Yusuke Hoshi, Kentarou Sawano, Yasuhiro Shiraki et al.

Citation: J. Appl. Phys. **111**, 073715 (2012); doi: 10.1063/1.3702464
View online: http://dx.doi.org/10.1063/1.3702464
View Table of Contents: http://jap.aip.org/resource/1/JAPIAU/v111/i7
Published by the American Institute of Physics.

Experimental and theoretical analysis of the temperature dependence of the two-dimensional electron mobility in a strained Si quantum well

Takahisa Tanaka,[1] Go Tsuchiya,[1] Yusuke Hoshi,[2] Kentarou Sawano,[2] Yasuhiro Shiraki,[2] and Kohei M. Itoh[1,a)]

[1]*School of Fundamental Science and Technology, Keio University, 3-14-1 Hiyoshi, Kohoku-ku, Yokohama, 223-8522, Japan*

[2]*Research Center for Silicon Nano-Science, Advanced Research Laboratories, Tokyo City University, 8-15-1 Todoroki, Setagaya-ku, Tokyo 158-0082, Japan*

(Received 12 December 2011; accepted 7 March 2012; published online 11 April 2012)

The temperature dependence of the mobility of the two-dimensional electron gas (2DEG) in a silicon quantum well strained by $Si_{0.7}Ge_{0.3}$ relaxed buffer layer is determined precisely by a mobility spectrum analysis. The 2DEG mobility is 2780 cm^2/V s at room temperature and, upon cooling, increases continuously to reach $\mu_{2DEG} = 7.4 \times 10^4$ cm^2/V s at 7 K. A back gate installed on the sample changes the 2DEG concentration n successfully to establish $\mu_{2DEG} \propto n^{1.4}$ at the constant temperature $T = 10$K, implying that the scattering at such low temperature is limited solely by the remote ionized impurity scattering. Based on this finding, theoretical analysis of the temperature dependence of μ_{2DEG} is performed based on the relaxation time approximation using 2DEG wavefunctions and subband structures determined self-consistently and including three major scatterings; by intravalley acoustic phonons, intervalley g-processes of longitudinal optical (LO) phonons, and remote ionized impurities. The calculation included only three fitting parameters, the shear deformation potential ($\Xi_u = 9.5$ eV), LO phonon deformation potential for g-process scattering ($D_0 = 9.0 \times 10^8$ eV/cm), and sheet density of remote ionized impurities that have been determined by quantitative comparison with our experimental results. The temperature dependence of μ_{2DEG} calculated theoretically show excellent agreement with experimentally determined μ_{2DEG}. © *2012 American Institute of Physics*. [http://dx.doi.org/10.1063/1.3702464]

I. INTRODUCTION

Reported values of the two-dimensional electron gas (2DEG) mobility μ_{2DEG} in Si/SiGe heterostructures have reached $2640 - 2900$ cm^2/V s at room temperature.[1–4] Such numbers are about four times higher than the mobility in the inversion layer in Si-MOSFET. The origin of the 2DEG mobility enhancement in Si/SiGe heterostructures is the change in the band structure by strain. The in-plane stress on the well imposed by the adjacent lattice-mismatched layer splits the sixfold-degenerate valleys of the silicon conduction band into twofold-degenerate and fourfold-degenerate.[5] With the in-plane tensile stress, the twofold-degenerate valleys become the bottom of the conduction band leading to a decrease in the conductivity effective mass and increase in transport relaxation time, i.e., enhancement of the electron mobility is expected. The conductivity effective mass become $0.195m_0$,[6] when the splitting energy is much higher than the thermal energy and electrons occupy only the twofold-degenerate valleys. However, such decrease in the conductivity effective mass enhances the mobility only by 30% and cannot be accounted for the four times enhancement reported before. Therefore, the increase of the transport relaxation time is the main factor contributing to the enhancement of the mobility by four times.[1–4]

The transport relaxation time is enhanced mainly by the suppression of f-process scattering, which is a scattering from one valley on a particular axis in k-space to one of other valleys on other axes in k-space. When the large enough in-plane tensile stress limits the electron occupations exclusively to the twofold-degenerate valleys situating on the same axis in k-space, f-process scattering is suppressed and phonon scatterings are allowed only for intravalley scattering and intervalley g-process scattering between the two occupiable valleys. In the past, it has been difficult to determine empirically the deformation potentials for such intravalley and intervalley g-process scattering since, for the case of Si-MOSFETs, intravalley, f-process and g-process coexist all together. Because independent determinations of the deformation potentials for the above mentioned three scattering mechanisms are very important for the device simulations of Si-MOSFETs, the present work demonstrate convincingly the determinations of the deformation potentials for intravalley scattering and intervalley g-process scattering in silicon using silicon quantum well (QW) strained by $Si_{0.7}Ge_{0.3}$ relaxed buffer layer in which all electrons are forced to occupy the twofold-degenerate valleys situating in the plane perpendicular direction.

The experimental method we have employed to probe purely the temperature dependence of the 2DEG mobility μ_{2DEG}, i.e., excluding the parallel conductions through the modulation-doped layer, buffer layer and substrate, is the maximum-entropy mobility spectrum analysis (ME-MSA).[7]

a)Author to whom correspondence should be addressed. Electronic mail: kitoh@appi.keio.ac.jp.

Using this technique, $\mu_{2DEG} = 2900\ \mathrm{cm}^2/\mathrm{Vs}$ at room temperature was probed recently.[4] The experimentally determined temperature dependence of the 2DEG mobility was compared quantitatively with theoretical calculation to check for the appropriateness of our theoretical model and to determine the shear and g-process of longitudinal optical (LO) phonon deformation potentials empirically. The calculation we employed involves the parabolic band with a variety of scattering mechanisms including phonon scattering with anisotropic deformation potentials proposed by Herring and Vogt in Ref. 8 and remote ionized impurity scattering.

II. EXPERIMENTS

A schematic diagram of our sample is presented in Fig. 1. The SiGe buffer layer consisting of a compositionally step-graded $Si_{1-x}Ge_x$ ($x = 0 \rightarrow 0.3$) layer (300 nm) and a uniform $Si_{0.7}Ge_{0.3}$ layer (1 μm) were grown by gas source molecular beam epitaxy (GS-MBE) on a p-type Si(001) substrate. After the planarization of the buffer layer by the chemical mechanical polishing,[9] the sample was loaded to GS-MBE again to form further a $Si_{0.7}Ge_{0.3}$ buffer layer (100 nm), a strained Si channel layer (15 nm), and a $Si_{0.7}Ge_{0.3}$ spacer layer (20 nm). Then, the sample was transferred to a solid source MBE to form a antimony (Sb) delta doped ($3 \times 10^{12}\ \mathrm{cm}^{-2}$) layer, a $Si_{0.7}Ge_{0.3}$ layer (40 nm), and a silicon cap layer (5 nm).

A mesa-type Hall bar was used for the ME-MSA and Hall effect measurements. The front electrodes were formed by ion implantation of phosphorous and evaporation of aluminum. An electrode to apply the back-gate voltages was formed by an AuGa evaporation. The electron Hall mobility and sheet carrier density of the whole structure were obtained by the conventional Hall effect using a magnetic field of 300 mT. The drift mobility, conductivity, and carrier density in each conduction layer were obtained by ME-MSA in the following way. The magnetic-field dependencies of the magnetoresistance (longitudinal resistance) and Hall resistance (perpendicular resistance) were measured in the range from 0 to 9 T with superconducting magnet at a fixed temperature. These values were converted into conductivity tensor components, $\sigma_{xx}(B)$ and $\sigma_{xy}(B)$, in accordance with the Hall bar geometry we employed. Then a maximum-entropy method was performed to obtain mobility spectrum.[7]

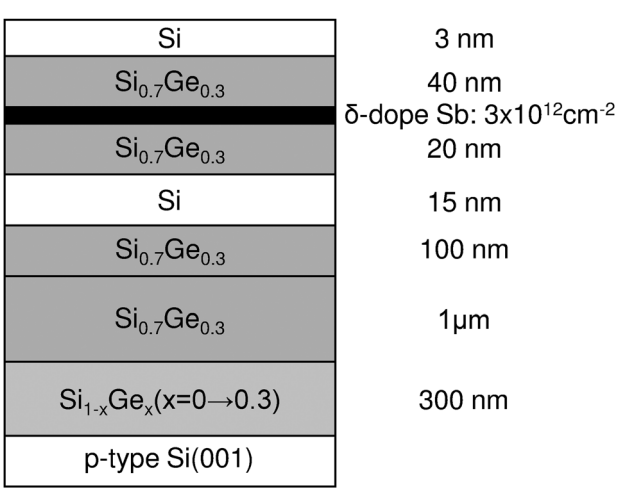

FIG. 1. A schematic diagram of the sample structure.

III. CALCULATION

A. Conduction band structure

The splitting energy of the twofold- and fourfold-valleys in a strained Si QW is proportional to the Ge content x of $Si/Si_{1-x}Ge_x$ heterostructures.[10] The electron occupancy of the twofold degenerate valleys is expected to be 100% at room temperature, when the Ge content becomes more than 20% in $Si/Si_{1-x}Ge_x$ heterostructures.[11] In the present work, we assume electrons exist exclusively in the twofold degenerate valleys even at room temperature because the Ge content of our sample is 30% leading to the splitting energy of $\sim$200 meV. Ellipsoidal parabolic bands are assumed. In all regions of Si and SiGe, the longitudinal effective mass m_l and transverse effective mass m_t we employed are $0.916m_0$ and $0.19m_0$ determined experimentally for Si,[12] which agrees with the theoretical consideration.[13]

B. Self-consistent solution

The Bloch function cannot be employed in the direction of the confinement, i.e., to the plane-perpendicular direction of the strained Si QW. Therefore, the wavefunctions and the subband energy levels in this direction were obtained by solving Schrödinger and Poisson equations self-consistently.[14–16] The Schrödinger equation is described by

$$\left[-\frac{\hbar^2}{2m_l}\frac{d^2}{dz^2} - e\phi(z) + V_b(z)\right]\zeta_i(z) = E_i\zeta_i(z), \qquad (1)$$

where $\phi(z)$ is the electrostatic potential, $V_b(z)$ is the potential energy associated with heterojunction discontinuity, E_i is the energy of the bottom of the ith subband, and $\zeta_i(z)$ is the wavefunction of the ith subband in the confinement direction. In accordance with the previous reports that calculated the energy difference of the conduction bands between a strained Si and SiGe,[13,17] the energy difference is assumed to be 200 meV. Thus, $V_b(z)$ is 0 meV in the quantum well and 200 meV outside. The Poisson equation is described by

$$\frac{d^2\phi(z)}{dz^2} = \frac{e}{\kappa}\left[N_A - N_h(z) + \sum_i n_i|\zeta_i(z)|^2\right], \qquad (2)$$

where κ is the dielectric constant, n_i is the electron density in ith subband, $N_h(z)$ is the concentration of free holes, and N_A is the background acceptor concentration. In the present work $N_A = 10^{16}\ \mathrm{cm}^{-3}$. The value of dielectric constant is $12.9\kappa_0$ for the SiGe layer[18] and $11.9\kappa_0$ for the Si layer.[19] In order to calculate n_i, the Fermi energy E_F has been determined to satisfy an experimentally obtained 2DEG carrier density n_{2DEG}. n_i is described by

$$n_i = \int n_v g_i(E) f_0(E) dE, \qquad (3)$$

where $n_v = 2$ is the number of degenerate valleys, $g_i(E)$ is the density of states of the ith subband, E is the energy of

electrons, and $f_0(E)$ is the Fermi-Dirac function. With this n_i the Poisson equation is solved.

C. Intravalley scattering

As proposed by Herring and Vogt,[8] the intravalley deformation potentials associated with longitudinal $\Xi_{\mathrm{LA}}(\beta_{//},\beta_z)$ and transverse acoustic phonons $\Xi_{\mathrm{TA}}(\beta_{//},\beta_z)$ are anisotropic and described by

$$\Xi_{\mathrm{LA}}(\beta_{//},\beta_z) = \Xi_d + \Xi_u \frac{\beta_z^2}{\beta_{//}^2+\beta_z^2}, \tag{4}$$

$$\Xi_{\mathrm{TA}}(\beta_{//},\beta_z) = \Xi_u \frac{\beta_{//}\beta_z}{\beta_{//}^2+\beta_z^2}, \tag{5}$$

where Ξ_d is the dilation deformation potential, Ξ_u is the shear deformation potential, $\beta_{//}$ and β_z are the in-plane and perpendicular components of the phonon wavevector, respectively. There are many theoretical and experimental reports on the values of Ξ_d and Ξ_u as summarized in Ref. 20. Although the values reported for Ξ_d by the same group scatters severely between -11.7 eV (Ref. 21) and 1.1 eV,[20] it has been shown convincingly in Ref. 20 that $\Xi_d = 1.1$ eV. Thus, the present work employs $\Xi_d = 1.1$ eV and treats Ξ_u as a parameter to be determined by comparison with the experiment below $T = 100$ K, since intervalley scattering can be negligible. The value of $\Xi_u = 9.5$ eV will be obtained based on the experimental results, which is in reasonable agreement with the previous experimental work.[22] When the intravalley scattering is treated as an elastic scattering, the transition probability from lth subband to mth subband including the anisotropy of the intravalley deformation potentials is described by[23]

$$W(\mathbf{k}',\mathbf{k}) = \frac{2\pi k_B T}{\rho\Omega\hbar u_s^2}\int_{-\infty}^{\infty} d\beta_z \Xi_i^2(\beta_{//},\beta_z) I_{ml}^2(\beta_z) \delta_{\mathbf{k}',\mathbf{k}+\beta_{//}}\delta[E(\mathbf{k}',m)-E(\mathbf{k},l)], \tag{6}$$

where

$$I_{ml}(\beta_z) = \left|\int dz \zeta_m^*(z)\zeta_l(z)\exp[i\beta_z z]\right|. \tag{7}$$

Here k_B is the Boltzmann constant, T is the temperature, ρ is the crystal density, Ω is the normalization volume, u_s is the sound velocity (u_{LA} or u_{TA}), $\Xi_i(\beta_{//},\beta_z)$ is the deformation potential ($i = $ LA or TA), $\mathbf{k}$ is the in-plane component of the electron wavevector in the initial state, and $\mathbf{k}'$ is the in-plane component of the electron wavevector in the final state. The integration over β_z indicates that the conservation of wavenumber is broken in the plane perpendicular direction. Integrating all the phonon wavenumbers, the transport relaxation time $\tau_{\mathrm{intra}}^l[E(\mathbf{k},l)]$ is described by

$$\frac{1}{\tau_{\mathrm{intra}}^l[E(\mathbf{k},l)]} = \frac{m_t k_B T}{(2\pi)^2\rho\hbar^3 u_s^2}\sum_m \int_{-\infty}^{\infty} d\beta_z I_{ml}^2(\beta_z) \times \int_0^{2\pi} d\theta \Xi_i^2(\beta_{//},\beta_z)\left(1-\frac{k'\cos\theta}{k}\right) U[E(\mathbf{k},l)-E(0,m)], \tag{8}$$

where θ is the scattering angle formed by $\mathbf{k}$ and $\mathbf{k}'$, and $U(E)$ is the step function. From the conservation of in-plane wavenumber and energy,

$$\beta_{//} = \sqrt{k^2 - 2kk'\cos\theta + k'^2} \tag{9}$$

$$k' = \left(\frac{2m_t}{\hbar^2}\right)^{0.5}\sqrt{E(\mathbf{k},l)-E(0,m)}. \tag{10}$$

D. Intervalley g-process scattering

Intervalley g-process scattering is treated in the conventional manner in which a constant deformation potential and constant phonon energy are assumed.[11,21] Similar to bulk Si, LO phonons are the major source of intervalley g-process scattering in a strained Si QW and its rate is described by[11]

$$\frac{1}{\tau_{\mathrm{inter}}^l[E(\mathbf{k},l)]} = \frac{m_t D_0^2}{2\rho\hbar^2\omega_0}\sum_m \int dz|\zeta_m(z)|^2|\zeta_l(z)|^2 \frac{1-f_0[E(\mathbf{k},l)\mp\hbar\omega_0]}{1-f_0[E(\mathbf{k},l)]} \times \left(N_0+\frac{1}{2}\pm\frac{1}{2}\right)U[E(\mathbf{k},l)-E(0,m)\mp\hbar\omega_0], \tag{11}$$

where $\hbar\omega_0$ is the energy of LO phonons and N_0 is the number of LO phonons. The first-order scattering by LA and TA phonons also exists. However the calculated first-order scattering rate using the method given in Ref. 24 and reported deformation potential values in Ref. 25 is much smaller compared to zeroth-order scattering by LO phonons. Thus, we consider only the zeroth-order scattering in the intervalley g-process. The LO deformation potential of g-process $D_0 = 9.0\times10^8$ eV/cm will be determined empirically using the experimentally obtained mobility at 300 K.

E. Remote ionized impurities scattering

Our sample has an antimony (Sb) doped layer at 20 nm away from the strained Si channel. Thus the remote ionized impurities scattering is taken into account. For calculation of

transport relaxation time, only intrasubband scattering is considered since intersubband scattering is negligible. In the Born approximation the transport relaxation time is described by[26]

$$\frac{1}{\tau^l_{\mathrm{RI}}[E(\mathbf{k},l)]} = \frac{m_t N_i}{2\pi\hbar^3}\int_0^{2\pi} d\theta |v_q(z_i)|^2 (1-\cos\theta), \tag{12}$$

where N_i is sheet density of ionized impurities, $q = k\sqrt{2(1-\cos\theta)}$ is momentum transfer, z_i is the position of ionized impurities and the factor $v_q(z_i)$ is the effective potential for electrons as in Ref. 26 with dielectric screening taken into account as in Ref. 27. To set the range of the QW as $0 < z < 20$ nm, $z_i = -20$ nm is obtained from the sample structure. In our calculation, $N_i = 8.0 \times 10^{11}$ cm^{-2} is used for sheet density of remote ionized impurities obtained by quantitative comparison with experiment together with Ξ_u.

F. Mobility calculation

The total transport relaxation time from lth subband is given by

$$\frac{1}{\tau^l(E)} = \frac{1}{\tau^l_{\mathrm{intra}}(E)} + \frac{1}{\tau^l_{\mathrm{inter}}(E)} + \frac{1}{\tau^l_{\mathrm{RI}}(E)}. \tag{13}$$

Under the relaxation-time approximation with the Boltzmann equation, the mobility is given by[26]

$$\mu = \frac{e}{m_t}\frac{\sum_l \int_{E_l}^{\infty} E\tau^l(E)\frac{\partial f_0(E)}{\partial E}dE}{n_v \sum_l \int_{E_l}^{\infty} E\frac{\partial f_0(E)}{\partial E}dE}. \tag{14}$$

In calculation, we considered up to the 9th subbands, because the same calculations with more than the 10th subband yields the same results.

IV. RESULTS AND DISCUSSION

Mobility spectra were obtained by the ME-MSA (Ref. 7) for the temperature between 7 K and 300 K. Figure 2 shows the magnetic field dependence of measured and fitted conductivity tensor components $\sigma_{xx}(B)$ and $\sigma_{xy}(B)$. Fittings have been performed using[7]

$$\sigma_{xx}(B) = \sum_i \frac{s(\mu_i)}{1+(\mu_i B)^2}, \tag{15}$$

$$\sigma_{xy}(B) = \sum_i \frac{s(\mu_i)\mu_i B}{1+(\mu_i B)^2}, \tag{16}$$

where $s(\mu_i)$ is the partial conductivity. Based on these excellent fittings, the mobility spectra shown in Fig. 3 have been obtained for the temperatures (a) 300 K and (b) 7 K. The negative mobility represents that carriers are electrons rather than holes. Between two peaks appearing in the negative mobility regions, it is reasonable to assume that the peak at the higher mobility represents the 2DEG mobility and the one on the lower mobility represents the parallel conduction of electrons through the Sb doped layer. Note that the integrated area under each peak represents the conductivity of the corresponding layer since the vertical axis is the partial conductivity. Figure 4 shows the temperature dependence of the carrier densities of the 2DEG ($n_{2\mathrm{DEG}}$, filled circles) and Sb-doped

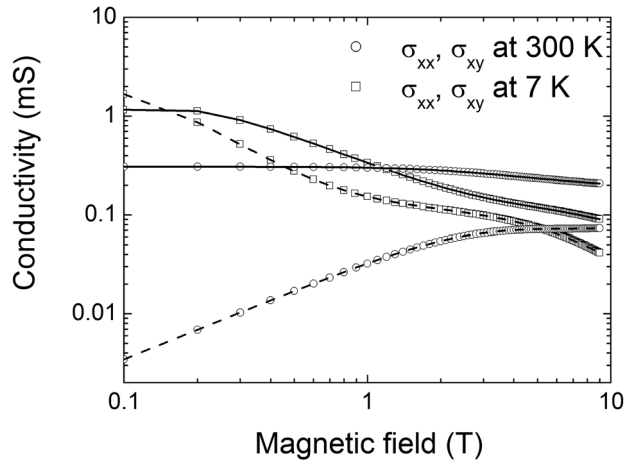

FIG. 2. Experimentally measured magnetic field dependence of $\sigma_{xx}(B)$ and $\sigma_{xy}(B)$ at 300 K (○) and 7 K (□) that have been fitted with Eq. (15) (solid curve) for $\sigma_{xx}(B)$ and Eq. (16) (dashed curve) for $\sigma_{xy}(B)$ shown in Ref. 7.

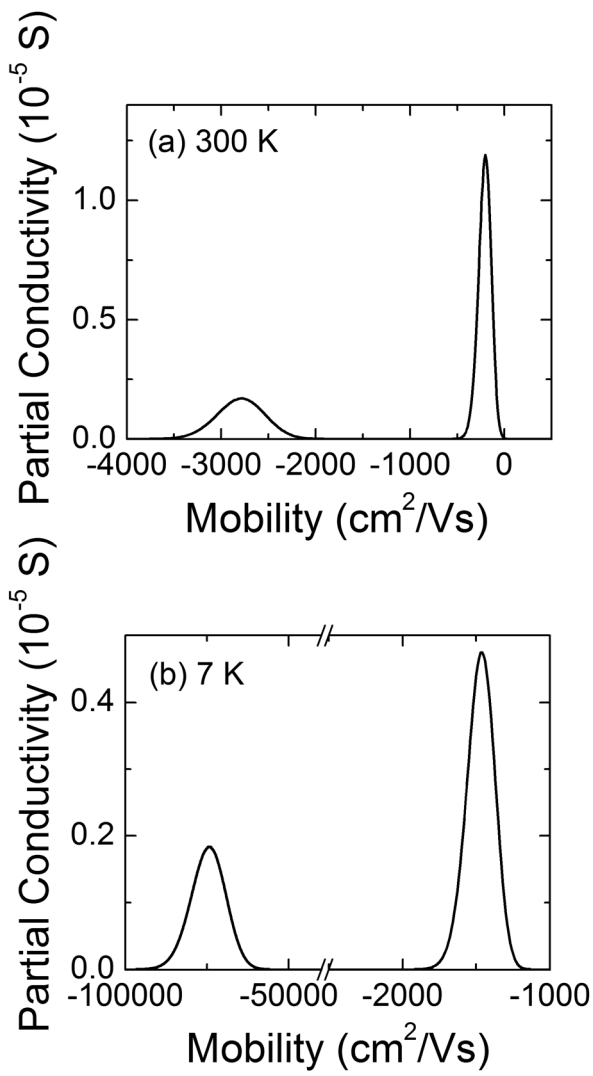

FIG. 3. Mobility spectra of Si/SiGe heterostructures at (a) 300 K and (b) 7 K.

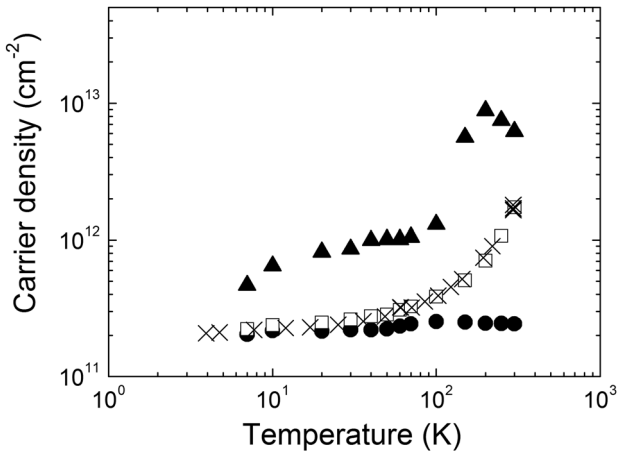

FIG. 4. Temperature dependence of 2DEG density (•), parallel electron density (▲), and averaged density (□) obtained by the mobility spectrum analysis and Hall density (×) obtained by Hall effect measurements.

(n_{Sb}, filled triangles) layers calculated from the conductivity and mobility of the each layer found in Fig. 3 using the simple relation $n = \sigma/q\mu$. Here the integration of the peak area was used to determine the conductivity and the peak mobility value was used as the representing mobility of the each layer. Figure 4 also shows the total carrier density n_{tot} of the structure (open squares) calculated based on the two-carrier layer Hall model,

$$n_{\text{tot}} = \frac{(n_{\text{2DEG}}\mu_{\text{2DEG}} + n_{\text{Sb}}\mu_{\text{Sb}})^2}{n_{\text{2DEG}}\mu_{\text{2DEG}}^2 + n_{\text{Sb}}\mu_{\text{Sb}}^2}, \tag{17}$$

where the measured density μ_{2DEG} and μ_{Sb} are taken from the peak positions of the ME-MSA, i.e., Fig. 3 for the given temperature. This total carrier density n_{tot} should be compared directly to the sheet carrier concentration n_{tot}' of the whole structure (crosses in Fig. 4) obtained from the conventional Hall effect measurements. It is clear that n_{tot} obtained by our ME-MSA and n_{tot}' obtained by the conventional Hall effect agree very well demonstrating the reliability and power of our ME-MSA method.

Figure 5 shows the temperature dependence of the mobility μ_{2DEG} and μ_{Sb}. Using the two-type carrier model,

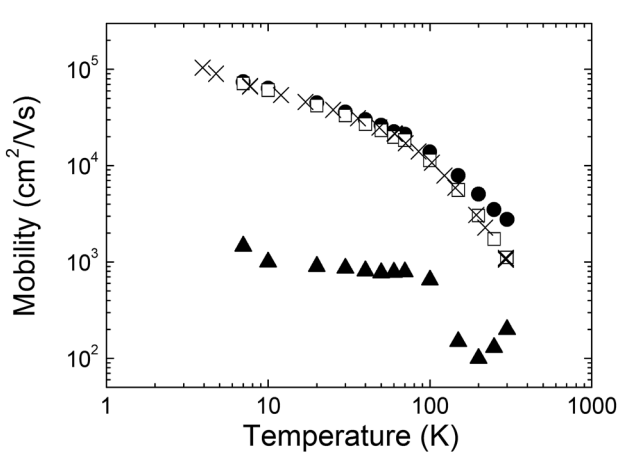

FIG. 5. Temperature dependence of 2DEG mobility (•), parallel electron mobility (▲), and averaged mobility (□) obtained by the mobility spectrum analysis and Hall mobility (×) obtained by Hall effect measurements.

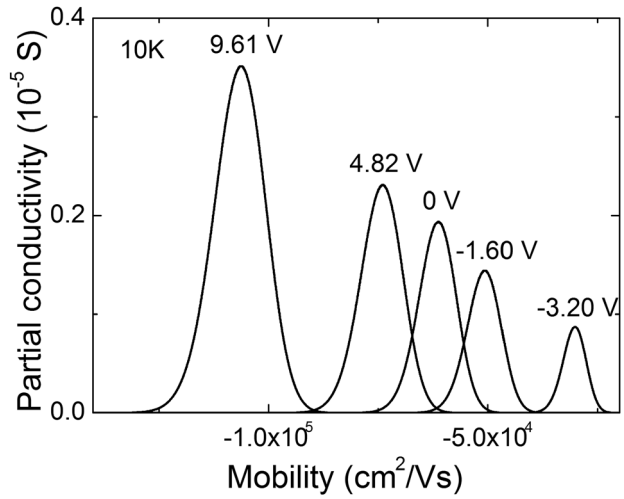

FIG. 6. Mobility spectra of 2DEG with different back-gate bias voltages indicated in the figures.

the averaged mobility of the whole structure μ_{ave} can be found as

$$\mu_{\text{ave}} = \frac{n_{\text{2DEG}}\mu_{\text{2DEG}}^2 + n_{\text{Sb}}\mu_{\text{Sb}}^2}{n_{\text{2DEG}}\mu_{\text{2DEG}} + n_{\text{Sb}}\mu_{\text{Sb}}}. \tag{18}$$

As shown in Fig. 5, the averaged mobility μ_{ave} found by ME-MSA (open squares) agrees very well with the mobility found by the conventional Hall effect (crosses), again, confirming the reliability of our method. The 2DEG drift mobility $\mu_{\text{2DEG}} = 2780\ \text{cm}^2/\text{Vs}$ obtained at room temperature is almost a factor of 3 larger than the Hall mobility 1070 cm^2/V s. This shows the importance of choosing ME-MSA to extract purely the nature of the 2DEG layer when other conduction layers (in our case the Sb doped layer) exist in parallel. Here the 2DEG mobility is almost equal to the record mobility 2900 cm^2/V s so far reported for strained Si.[4]

In order to further probe the scattering mechanisms of the 2DEG, we have fabricated a back-gate that allows for tuning the carrier concentration of the 2DEG layer at low temperatures. Figure 6 shows mobility spectra of 2DEG with different back-gate bias voltages recorded at $T = 10$ K. The shift of the

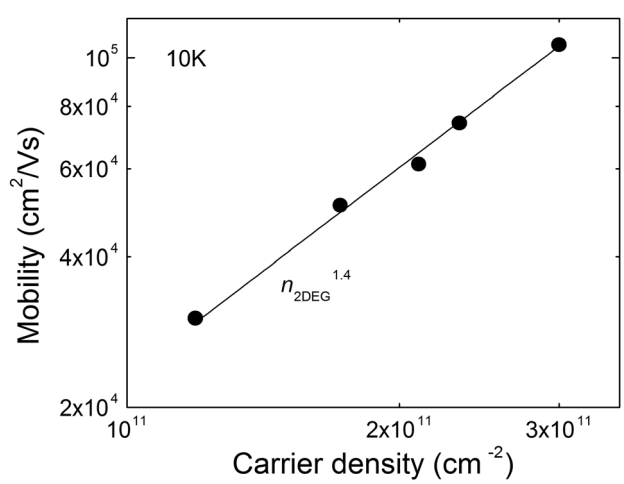

FIG. 7. 2DEG density (•) dependence of mobility with a variety of back gate voltages at $T = 10$ K. A fit to 2DEG mobility yields power dependence n_{2DEG}^{α}.

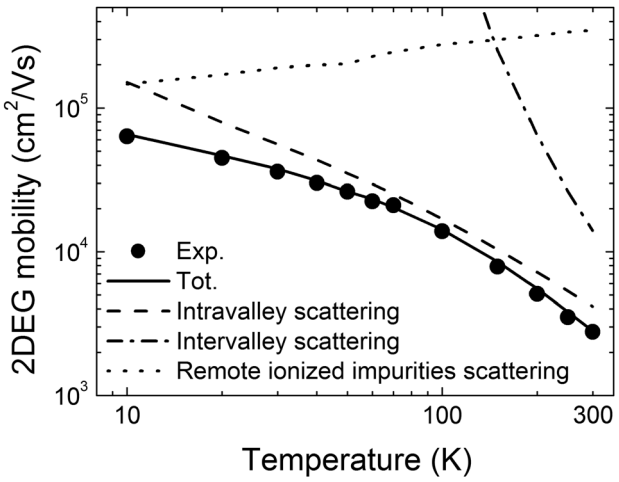

FIG. 8. Temperature dependence of 2DEG mobility (•) obtained by mobility spectrum analysis. Theoretical curve is shown for the total mobility including three scattering mechanisms, the intravalley scattering, intervalley scattering, and remote ionized impurities scattering. The theoretical mobility limited by each of the scattering mechanisms is also shown.

spectrum indicates successful modulation of the 2DEG mobility and conductivity. Figure 7 shows the mobility of 2DEG (μ_{2DEG}) as a function of the 2DEG carrier density (n_{2DEG}). The back-gate allows for the significant change of the 2DEG mobility and density in the range $\mu_{2DEG} = 30000 - 106000\ \mathrm{cm^2/Vs}$ and $n_{2DEG} = 1.2 - 3.0 \times 10^{11}\mathrm{cm}^{-2}$. In this entire rage, the 2DEG mobility is found to show $\mu_{2DEG} \propto n_{2DEG}^{\alpha}$ with $\alpha = 1.4$, the dependence expected for 2DEG at low temperatures[28] and α is very close to $\alpha = 1.5$ for the case when the remote ionized impurity scattering is limiting μ_{2DEG}.[14] Therefore, it is sufficient to consider only the phonon scattering and remote ionized impurities scattering in our calculation of the temperature dependence of 2DEG mobility.

Figure 8 shows the experimentally obtained 2DEG mobility (open circles), calculated mobility limited by intravalley scattering (dashed line), calculated mobility limited by intervalley scattering (chain line), calculated mobility limited by remote ionized impurities scattering (dotted line), and calculated mobility including all the three scattering (bold line). An excellent agreement is found between the experimental and calculated mobility with the empirically determined shear deformation potential ($\Xi_u = 9.5$ eV) and longitudinal optical phonon deformation potential for g-process scattering ($D_0 = 9.0 \times 10^8$ eV/cm). These values are expected to be valid in calculations not only for strained Si grown on $Si_{1-x}Ge_x$ with $x = 0.3$ but also unstrained Si, i.e., applicable for device modeling of industrially produced Si MOSFET.

V. CONCLUSION

By the maximum-entropy mobility spectrum analysis and numerical calculations, we have studied transport properties of 2DEG in the Si quantum well strained by a $Si_{0.7}Ge_{0.3}$ relaxed buffer layer. The emphasis has been placed on manifestation of contribution of each scattering mechanism to experimentally determined 2DEG mobility. The shear deformation potential ($\Xi_u = 9.5$ eV) and longitudinal optical phonon deformation potential for g-process scattering ($D_0 = 9.0 \times 10^8$ eV/cm) determined in this work shall be useful to determine other unknown deformation potentials such as the f-process scattering in Si-MOSFET.

ACKNOWLEDGMENTS

We would like to thank Professor Shinichi Takagi for fruitful discussions. This work was supported in part by Grant-in-Aid for Scientific Research and Project for Developing Innovation Systems by MEXT, FIRST, and Keio G-COE. The work at Tokyo City University has been supported in part by Strategic Advancement of Research Infrastructure for Private Universities 2009-2013, and a Grant-in-Aid for Scientific Research, and the Industrial Technology Research Program from NEDO.

[1]S. F. Nelson, K. Ismail, J. O. Chu, and B. S. Meyerson, Appl. Phys. Lett. **63**, 367 (1993).
[2]K. Ismail, S. F. Nelson, J. O. Chu, and B. S. Meyerson, Appl. Phys. Lett. **63**, 660 (1993).
[3]L. Di Gaspare, K. Alfaramawi, F. Evangelisti, E. Palange, G. Barucca, and G. Majni, Appl. Phys. Lett. **79**, 2031 (2001).
[4]M. Myronov, K. Sawano, K. M. Itoh, and Y. Shiraki, Appl. Phys. Express **1**, 021402 (2008).
[5]G. Abstreiter, H. Brugger, T. Wolf, H. Jorke, and H. K. Herzog, Phys. Rev. Lett. **54**, 2441 (1985).
[6]S. Q. Murphy, Z. Schlesinger, S. F. Nelson, J. O. Chu, and B. S. Meyerson, Appl. Phys. Lett. **63**, 222 (1993).
[7]S. Kiatgamolchai, M. Myronov, O. A. Mironov, V. G. Kantser, E. H. C. Parker, and T. E. Whall, Phys. Rev. E **66**, 036705 (2002).
[8]C. Herring and E. Vogt, Phys. Rev. **101**, 944 (1956).
[9]K. Sawano, S. Koh, Y. Hirose, T. Hattori, K. Nakagawa, and Y. Shiraki, Appl. Phys. Lett. **82**, 412 (2003).
[10]C. Euaruksakul, Z. W. Li, F. Zheng, F. J. Himpsel, C. S. Ritz, B. Tanto, D. E. Savage, X. S. Liu, and M. G. Lagally, Phys. Rev. Lett. **101**, 147403 (2008).
[11]S. Takagi, J. L. Hoyt, J. J. Welser, and J. F. Gibbons, J. Appl. Phys. **80**, 1567 (1996).
[12]J. C. Hensel, H. Hasegawa, and M. Nakayama, Phys. Rev. **138**, A225 (1965).
[13]M. M. Rieger and P. Vogl, Phys. Rev. B **48**, 14276 (1993); **50**, 8138(E) (1994).
[14]D. Monroe, Y. H. Xie, E. A. Fitzgerald, P. J. Silverman, and G. P. Watson, J. Vac. Sci. Technol. B **11**, 1731 (1993).
[15]S. Takagi, A. Toriumi, M. Iwase, and H. Tango, IEEE Trans. Electron Devices **41**, 2357 (1994).
[16]F. Monsef, P. Dollfus, S. G. Retailleau, H. J. Herzog, and T. Hackbarth, J. Appl. Phys. **95**, 3587 (2004).
[17]F. Schäffler, Semicond. Sci. Technol. **12**, 1515 (1997).
[18]R. Ahuja, C. Persson, A. F. de Almeida, C. M. Araujo, and B. Johansson, J. Appl. Phys. **93**, 3832 (2003).
[19]K. V. Rao and A. Smakula, J. Appl. Phys. **37**, 2840 (1966).
[20]M. V. Fischetti and S. E. Laux, J. Appl. Phys. **80**, 2234 (1996).
[21]M. V. Fischetti and S. E. Laux, Phys. Rev. B **48**, 2244 (1993).
[22]J. S. Lim, X. Yang, T. Nishida, and S. E. Thompson, Appl. Phys. Lett. **80**, 073509 (2006).
[23]M. Lundstrom, *Fundamentals of Carrier Transport* (Cambridge University Press, 2000), p. 99.
[24]F. Monsef, P. Dollfus, S. Galdin, and A. Bournel, Phys. Rev. B **65**, 212304 (2002); Phys. Rev. B **67**, 059903(E) (2003).
[25]P. Dollfus, J. Appl. Phys. **82**, 3911 (1997).
[26]T. Ando, A. B. Fowler, and F. Stern, Rev. Mod. Phys. **54**, 437 (1982).
[27]M. V. Fischetti, J. Appl. Phys. **89**, 1232 (2001).
[28]K. Ismail, M. Arafa, F. Stern, J. O. Chu, and B. S. Meyerson, Appl. Phys. Lett. **66**, 842 (1995).